Solar beam attenuation experiments-Abu Dhabi

Zaid Tahboub, Abdul Aziz Al Obaidli, Francisco Luque, Ibon Salbidegoitia, Olivier Farges, Zhor Hassar, Armel Oumbe, Norbert Geuder, Olaf Goebel

Solar Beam Attenuation Experiments – Abu Dhabi

Zaid M. Tahboub[1], Abdul Aziz Al Obaidli[2], Francisco Luque[3], Ibon Salbidegoitia[4], Olivier Farges[5], Zhor Hassar[5], Armel Oumbe[5], Norbert Geuder[6] and Olaf Goebel[7]

[1] Solar Eng., Masdar Power, P.O.Box 54115, Abu Dhabi, UAE, Phone: +971-2-653-2042, E-Mail: ztahboub@masdar.ae.

[2] Process Eng., Shams Power Company, P.O.Box 54115, Abu Dhabi, UAE, Phone: +971-50-950-3313.

[3] Senior CSP Eng., Masdar Power, P.O.Box 54115, Abu Dhabi, UAE, Phone: +971-2-653-2077.

[4] CSP Eng., Torresol Energy, Avda. Zugazarte, 61, C.P. 48930, Las Arenas, Bizkaia, Spain.

[5] Total Gas & Power, R&D – Concentrated Solar Technologies, France.

[6] CSP Services, Paseo de Almería 73, 04001 Almería, Spain, Phone: +34-950-274-350.

[7] Prof. Dr., Hochschule Hamm Lippstadt, Marker Allee 76-78, 59063 Hamm, Phone: +49-2381-878-427.

Abstract

In SolarPACES 2011, Masdar Power presented the two proposed experimental setups and the methodology to quantify the solar beam attenuation due to aerosol particles in the air. Both test setups have been built and commissioned and have been running. An update about the experimental setups and the associated challenges are presented in this paper. Moreover, we present the proposed methods that we plan to use in order to overcome these challenges.

Keywords: CSP, attenuation, solar tower, central receiver, aerosol, dust.

1. Introduction

Having been in operation for almost a year, Gemasolar's[1] remarkable performance is paving the way towards the widespread of the central tower (CT) concentrated solar power (CSP) technology. In contrary to other solar energy technologies like PV or parabolic troughs, the thermal receiver in a CT plant may be several hundred meters away from the reflecting heliostat mirrors. Therefore, the solar beam has a notably longer path length to pass until it reaches the thermal receiver and thus is subject to higher attenuation by scattering and extinction due to aerosols and water vapor. Furthermore, the path is situated in the lower atmospheric layers where increased attenuation is expected. So far only sparse information is available on atmospheric attenuation especially under conditions commonly prevailing in this region. Two experiments are being conducted to determine attenuation quantity and occurrence frequency of common atmospheric conditions in order to judge its influence on the performance of the CT technology [1].

Two different tests were setup in two different locations and both have been installed and commissioned. A description of the setups and the rationale behind each were described in details by Alobaidli et al [1]. These setups will help us build a model that predicts the atmospheric attenuation that the solar radiation may undergo during its travel between a heliostat and the thermal receiver at the top of the tower in a CT plant. In the following sections, the two setups and the related challenges and ways to tackle them will be explained.

2. Horizontal Attenuation – Swaihan Experiment

2.1 Test Setup

The proposed setup was built and commissioned in the last quarter of 2011 and a schematic diagram of the setup is shown in figure 1-a. In this test setup, the beam radiation is reflected by a heliostat horizontally towards four inline podiums (figure 1-c) designed to welcome a portable pyrheliometer (figure 1-e). Close to

[1] The concentrated solar power plant located in Fuentes de Andalucía (Seville) - Spain, a property of Torresol Energy (a joint venture between Masdar – Abu Dhabi's clean energy initiative and SENER).

the heliostat, measurements of Direct Normal Irradiance (DNI) and visibility are made (figure 1-b and d). These measurements serve as inputs to simulate the propagation of the radiation from the heliostat to the podiums - using a ray tracing code - (the circumsolar ratio is firstly computed using a radiative transfer code). The reflected beam radiation is measured at different distances from the heliostat (100, 400, 700 and 1000 m) using a portable pyrheliometer (figure 1-e). The values of the measured beam are then compared to simulated values (with zero attenuation assumed) (figure 1-f) and the atmospheric attenuation can then be determined. On the other hand, this atmospheric attenuation is also estimated with an analytical model. The comparison of both attenuations will help to verify the consistency of the experiment. Having an accurate model of irradiance attenuation from heliostat to tower is of great interest for the monitoring of flux reaching the top of the tower in an operational CT plant.

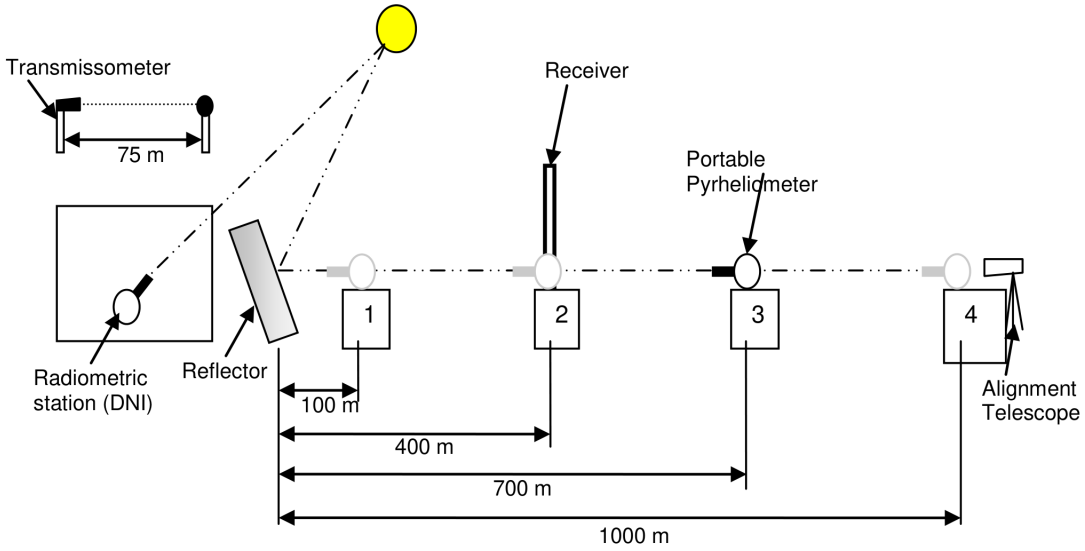

(a)

(b)

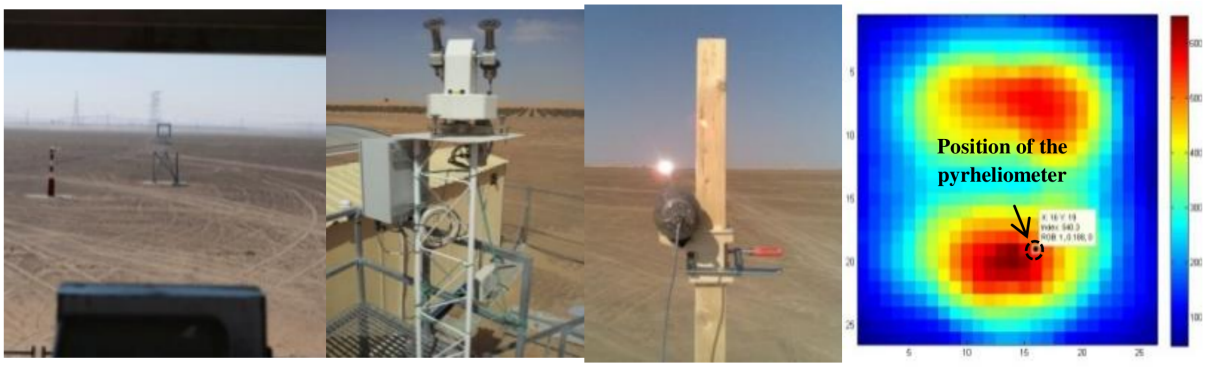

(c) (d) (e) (f)

Figure 1: (a) Schematic diagram of the test setup of Swaihan. (b) Heliostat, transmissometer receiver, reference pyrheliometers. (c) Podiums as seen from the heliostat. (d) Reference pyrheliometers. (e) Portable pyrheliometer measuring reflected beam. (f) Simulated flux distribution map at 100 m for DNI 800 W/m^2, assuming zero attenuation.

2.2 Modelling of the Atmospheric Attenuation from the Mirror to the Target

In order to model the atmospheric attenuation, an analytical parameterization of propagation of clear-sky direct irradiance, within 100 m above the surface is proposed. This parameterization is based on the resolution of radiative transfer equation by the libRadtran (www.libradtran.org). The inputs of the parameterization are the DNI at a given position (at the radiometric station) and the visibility of the air (*vis*).

2.2.1 Parameterization of the DNI Attenuation from Heliostat to the Top of a CT

During its progress through the atmosphere, solar radiation is intercepted by a large number of particles ranging in size from one-tenth of a nanometer (molecules) to a few centimeters (precipitating particles). Electromagnetic waves then undergo scattering phenomena (reflection, refraction and diffraction) causing a dispersion of radiation in all directions, and absorption (part of the incident energy is converted to another form of energy). All these phenomena are often modelled by the means of radiative transfer codes.

The goal here is to model the propagation of irradiance in all directions. In order to study the direction dependence of irradiance propagation in the layer between the ground and 100 m, we compare - using libRadtran - the attenuation of DNI for the same distance of propagation for various solar zenith angles (θ), and elevation above the surface (z) ranging between 0 and 100 m: the variation obtained is almost less than 1%. It is therefore assumed that whatever the direction, for a given atmosphere, the attenuation of the irradiance (*Att*) depends only on the distance travelled by the radiation ($d = d1-d0$) and the visibility (*vis*):

$$DNI(d1) = DNI(d0) * Att(vis, d1-d0) \qquad (1)$$

where *d0* and *d1* are expressed in km. $d1 > d0$. Practically, *d0* can be the position of the receptor, and *d1* the position at which one wants to know the irradiance.

Based on the above comparison, we assume that the atmosphere is homogeneous in the layer 0 – 100 m. Visibility (*vis*) is used in the equation to characterise the atmospheric state and it is measured by the transmissiometer located on site.

For practical reasons, it is convenient to have an analytical parameterization: it allows easy implementation and rapid calculation of the converted irradiance. We propose a parameterization which estimates the attenuation of DNI from the visibility:

$$DNI(d1) = DNI(d0)\ a^{-(d1-d0)} \qquad (2)$$

The parameter *a* have been empirically found with libRadtran simulations and are set as follows:

vis < 3 km, *a* = 2.00

3 km < *vis* < 6 km, *a* = 1.55

6 km < *vis* < 11 km, *a* = 1.32

11 km < *vis* < 20 km, *a* = 1.18

20 km < *vis* < 40 km, *a* = 1.09

40 km < *vis* < 70 km, *a* = 1.06

vis ≥ 70 km, *a* = 1.04 *(3)*

2.2.2 Comparison of the Analytical Model to the Radiative Transfer Code - libRadtran

In order to assess the performances of the proposed parameterization, its outputs are compared to those of libRadtran. A Monte-Carlo technique is applied to randomly select 5000 sets within the 3D-space defined by discrete values of solar zenith angle (θ), visibility (*vis*) of the air and elevation above the surface (z). Uniform distributions are used with the ranges 10° to 80° for solar zenith angle, 2 km to 100 km for *vis*, and 10 m to 100 m for *z*. Hence, the path of the radiation (*d*) is given by

$$d = z / \cos(\theta) \qquad (4)$$

Therefore, in these comparisons, *d* is rarely higher than 0.5 km and can reach large values only in large θ which correspond to low DNI values. For each set of θ, *vis* and *z*, libRadtran computes *DNI* at two elevations – 0 km (*d0*) and the randomly selected one (*d1*). The *DNI(d0)* and the corresponding visibility are used to compute *DNI(d1)* with the parameterization, as described above (equation *2*). The comparison shows that outcomes of the parameterization are close to those of libRadtran: mean absolute error (MAE) and root mean square deviation (RMSD) on *DNI* are often less than 2 W/m^2. However, the performance of the parameterization decreases when the distance from the reference increases. The linear regression of MAE and RMSD are given by:

RMSD = 7.1 * distance + 0.3 (W/m2) *(5)*

MAE = -9.9 * distance + 1.0 (W/m2) *(6)*

With distance in km. This predicts errors less than 10 W/m^2 for distances up to 1 km.

2.3 Data Analysis and Sources of Uncertainty

As mentioned in section 2.1, a ray tracing code is used to simulate the reflected flux assuming no attenuation. The reflected flux measured using the portable pyrheliometer is then compared with specific points on the simulated flux map (as depicted in figure 1-f). These points represent the position of the pyrheliometer with reference to the target at the time of measurement.

After conducting preliminary analysis on the collected data using the above method, it was found that the simulated flux is producing lower values than that of the measured flux. Different reasons were identified as

possible causes for the underestimation of the ray tracing code and can be summarized in the following points:

1- A change in the mirror shape:

As was described by Alobaidli et al [1], the mirror shape was measured by defining a mesh on the mirror facet with as many points as the experiment requires using a software application developed by Torresol. Laser techniques were then used to obtain the normal vectors at defined points on the mirror facet. This was done in a laboratory under constant temperature. This mirror shape was used as an input for the ray tracing code. It is believed that the shape of the mirror is dependent on the temperature and is changing at the time of conducting the experiment. In order to overcome this issue, on site mirror shape measurements will be conducted using optical techniques. Moreover, a different mirror that has more suitable thermal characteristics may be tested and used.

2- Tracking error:

The heliostat used in this experiment corrects its position when the difference between the real and ideal tracking angle is equal to or more than 0.05^{o}. This results in the movement of the reflected flux along the target at the time when the heliostat is stationary. In the ray tracing code the ideal position of the mirror was used to reduce the computation time. Alobaidli [2] showed that the uncertainty in the results due to the tracking error is significant and is dependent on the distance from the heliostat. To tackle this problem, the real position of the heliostat will be used as an input for the ray tracing code. This will be achieved by logging the real azimuth and zenith of the mirror facet and using them as an input for the ray tracing code.

3- Number of rays and the resolution of the target used in the ray tracing code:

Both the number of rays and the resolution of the target used in the ray tracing code have an effect on the values of the simulated flux. Optimizing the number of rays and the resolution of target is undergoing. An example of the resolution of target can be seen in figure 2. The selection of the target resolution will take into consideration the area of the pyrheliometer sensor to make sure that the resolution used has a sound physical meaning.

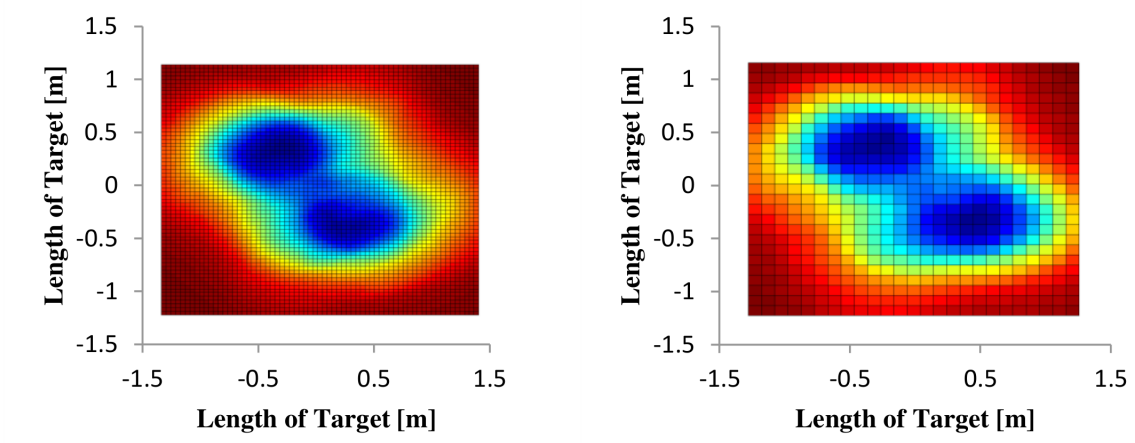

Figure 2: (a) Target at 100m, CSR=0.4, DNI=1000 W/m^2, Sun points 700, target points 70. (b) Target at 100m, CSR=0.4, DNI=1000 W/m^2, Sun points 1000, target points 28.

It is worth mentioning that Alobaidli [2] studied in details the sources of uncertainties associated with this setup. The main sources and the ones that can be fairly easily accounted for are being addressed at this stage and are described in this paper. An example of a source of error that is not being addressed at this stage is the reduction in the reflected irradiance due to the mirror size (not seeing a complete sun at distances greater than ~140 m from the mirror) which affects the accuracy of the pyrheliometer.

2.3.1 Ray Tracing Calculations with EDStar

Another approach is explored: modeling of our experimentation using EDStar (www.starwest.ups-tlse.fr). EDStar (numerical Environment of Development for Statistical Radiative simulation) is a development environment helping to conceive codes from existing pre-build parts with new computation tools (massive parallelization, automatic calculus of sensitivities, acceleration of the ray tracing in complex geometry). It has been developed for the simulation of corpuscular transport phenomena, in particular radiative transfer.

In order to obtain a satisfactory degree of precision:

1. We have reproduced the experimental set-up with EDStar environment. This consists in a mirror tracking the sun and reflecting the beam irradiance to the targets. This is represented in the figure 3.

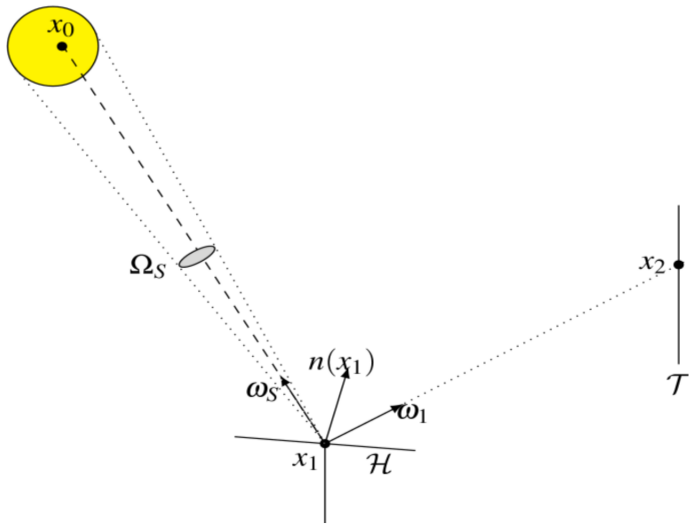

Figure 3: Set-up modeled with the EDStar ray-tracing code.

2. As the mirror was presumed to be flat, but shows some surface deformations, we facetize the heliostat according to data collected during the characterization of the mirror. This refinement gives us a great precision as the reflective surface is subdivised in 4489 subareas. This allows taking into account the real orientation of the surface normal vector at a specific position on the mirror.

3. As we want to compare experimental data with simulated results, we consider pyrheliometer specification and especially acceptance angle. To do so, we introduce a condition to exclude rays hitting target with acceptance angle greater than 5 degrees.

4. In order to compute automatically the flux map for all the measurements time-series, we add a module which convert the date (day and hour) and latitude to set the sun position (azimuth and hour angle).

The inputs of the obtained ray-tracing code are: distance between the heliostat and the target, direct normal irradiance (DNI), date and latitude.

3. "Vertical" Attenuation - Jabal Hafeet Experiment

3.1 Test Setup

Jabal Hafeet is the highest mountain is UAE. In this experiment, four pyrheliometers are located at different altitudes[2] from 340 m to more than 1000 m above mean sea level to continuously record DNI with high precision (pyrheliometers are cleaned daily). Here the attenuation of the direct solar beam component is

[2] Installation was done by CSP Services.

determined for different altitudes. This experiment yields important information on the altitudinal distribution of attenuating aerosols, water vapor, etc., as well as on the temporal distribution, range and occurrence frequencies over the year. This can serve to improve aerosol modeling and estimate expectable annual CT plant gains.

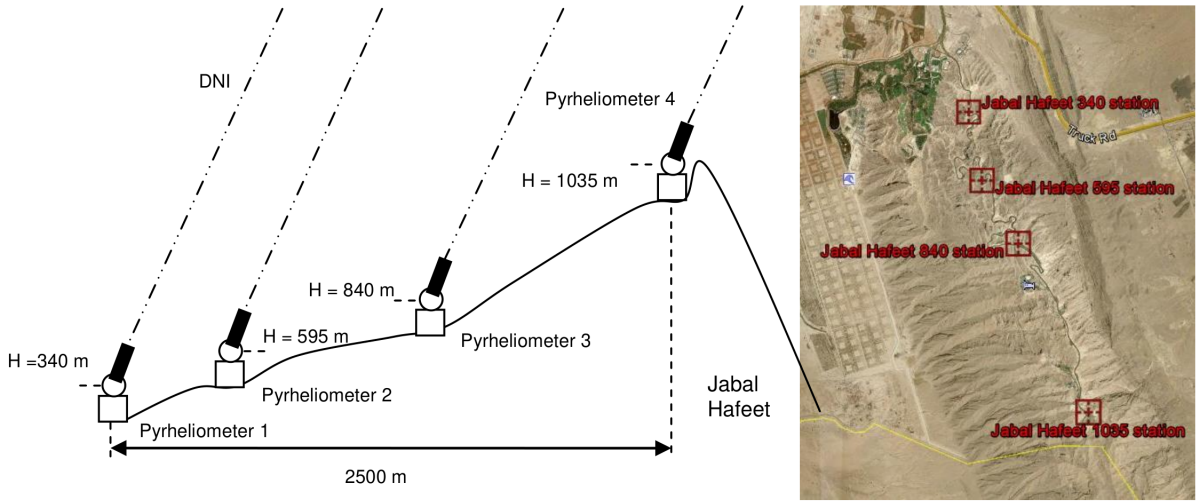

(a) (b)

Figure 4: (a) Schematic diagram of the test setup of Jabal Hafeet. (b) Aerial view of the four stations on Jabal Hafeet (Google Earth).

The dataset is temperature corrected and calibration adjusted before attempting to analyze the data. The calibration of the four pyrheliometers was carried out by placing all four it the top station for several days and then finding a calibration adjustment factors for each to gain exactly coinciding readings (depicted in figure 5).

(a) **(b)**

Figure 5: (a) fine calibration of the four pyrheliometers against each other before the experiment started (b) station at 1035 m during the calibration.

3.2 Data Analysis and Sources of Uncertainty

Comparing the DNI readings of the different stations in Jabal Hafeet should be carried out with precaution. The fact that the four stations differ in 1- the horizontal position and 2- the surrounding landscape may cause different blocking and shading schemes which will produce outlier data points that needs to be identified and deleted before concluding values of attenuation. In our analysis of the outliers we assume a homogeneous distribution of aerosols above Jabal Hafeet.

Outlier data points may arise from different reasons such as:

1- Intermittent clouds that lead to shade some pyrheliometers and not the others.
2- Blocking of the sun by nearby objects (due to the surrounding landscape) or passing by objects. For example the station at 340 m is blocked by the mountain in the afternoon. Another example would be in case the sun is low and a big vehicle (e.g. a tourists' bus) passes next to the pyrheliometer and blocks the sun.

To give an example of the outliers that can result, a scatter plot of the data gathered from 28th Jan to 16th Feb, 2012 is shown in figure 6. Here the DNI measured at altitude of 340 m is plotted against that measured at 1035 m. It is noticed that some points represent times when DNI_{340} is higher than DNI_{1035}. These points are most probably created as a result of intermittent clouds covering the station at 1035 m causing lower DNI values at 1035 m than that at 340 m (defined as region 1 which are points above the DNI_{340}=DNI_{1035} line indicated in blue). These values are not connected to atmospheric attenuation and thus are considered as outliers and should be deleted.

The difficulty arises when we try to identify outliers in region 2. Points in region 2 can be either cause by attenuation due to aerosols or by shading of the station at 340 m. In the case of attenuation, the position of the data on the scatter plot will vary depending on the composition of the atmosphere (i.e. the aerosol content).

One method that we are currently exploring to enable us to identify outlier points in region 2 is to use satellite images and identify cloud coverage above Jabal Hafeet. This will enable us to delete data points when Jabal Hafeet is covered by intermittent clouds.

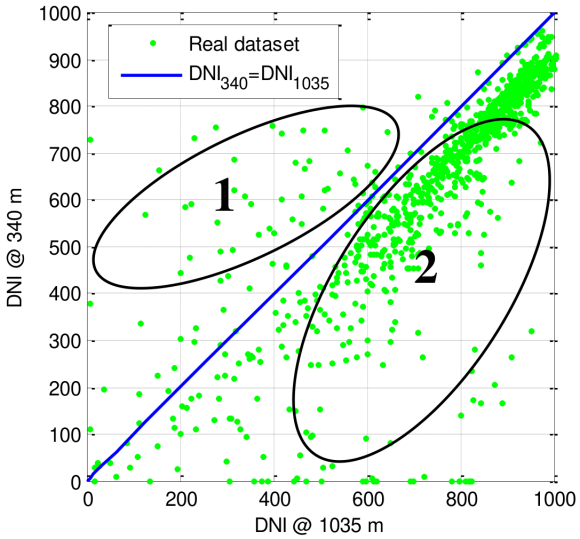

Figure 6: Plot of data set gathered from 28th Jan to 16th Feb, 2012.

Acknowledgements

Authors would like to extend their appreciation to Mr. Jerry Tabuan who made a great effort in helping us with running the experimental setups and taking measurements.

References

[1] SolarPACES 2011, Beam Attenuation Test for Solar Power Tower, O. Goebel, F. Luque, A. Alobaidli and I. Salbidegoitia.

[2] Master's Thesis, Aachen, April 2012, Atmospheric Attenuation Test, A.A AlHammadi.